Bulletin of the Seismological Society of America, Vol. 107, No. 5, pp. 2342–2352, October 2017, doi: 10.1785/0120160278

Seismic-Hazard Assessment over Time: Modeling Earthquakes in Taiwan

by Chung-Han Chan, Yu Wang, Yu-Ju Wang,* and Ya-Ting Lee

Abstract To assess the seismic hazard with temporal change in Taiwan, we developed a new approach which combines both the Brownian passage time (BPT) model and the coulomb stress change, and implements the seismogenic source parameters by the Taiwan Earthquake Model. The BPT model was adopted to describe the rupture recurrence intervals of specific fault sources together with the time elapsed since the last fault rupture to derive their long-term rupture probability. We also evaluated the short-term seismicity rate change based on the static coulomb stress interaction between seismogenic sources. By considering these time-dependent factors, our new combined model, relative to a time-independent model, suggests an increased long-term seismic hazard in the vicinity of active faults along the western coastal plain and the Longitudinal Valley, where active faults have short recurrence intervals and long elapsed time since their last ruptures and/or short-term elevated hazard levels right after the occurrence of large earthquakes due to the stress triggering effect. The stress enhanced by the 6 February 2016 M_L 6.6 Meinong earthquake also significantly increased the rupture probabilities of several neighboring seismogenic sources in southwestern Taiwan and raised the hazard level for the near future. Our approach drew upon the advantage of incorporating both long- and short-term models to provide time-dependent earthquake probability constraints. This new model provides more insight than any other models for Taiwan. Thus, it offers decision makers and public officials an adequate basis for rapid evaluations of consequent hazards and for responses to future emergency scenarios such as victim relocation and sheltering.

Introduction

A probabilistic seismic-hazard assessment (PSHA) represents the probability of exceedance of ground shaking during an assumed period (Cornell, 1968), which is useful for seismic-hazard mitigation and risk management (McGuire, 2001). A traditional PSHA assumes that the occurrence of earthquakes simply follows the Poisson procedure (Merz and Cornell, 1973; Ang and Tang, 1975; Cornell and Winterstein, 1986) and that earthquakes are independent of one another. Thus, the hazards from foreshocks and aftershocks are excluded from this assessment (e.g., Gardner and Knopoff, 1974).

The time-independent assumption in PSHA has been questioned, since earthquakes are temporally and spatially dependent (Harris, 1998, and references therein). For example, in 2010, the Darfield mainshock caused a sequence of aftershocks in New Zealand, including the 2011 M_w 6.2 Christchurch aftershock, that caused more damage in downtown Christchurch than the 2010 M_w 7.1 Darfield mainshock. The disadvantage of the time-independent PSHA was revealed in the Darfield sequence in New Zealand (Chan *et al.*, 2012).

In addition, a strong foreshock could trigger a mainshock event that generates considerable hazards. The Kumamoto earthquake sequence in 2016 is one of these foreshock–mainshock examples, in which an M_w 6.2 foreshock occurred in western Kyushu, Japan, on 14 April 2016, triggering the disastrous M_w 7.1 mainshock on 16 April. These examples highlight the importance of re-evaluating seismic hazards immediately following large earthquakes.

The above-mentioned observations offered motivation for researchers to propose time-dependent approaches for earthquake forecasting (e.g., Omi *et al.*, 2015; Rhoades *et al.*, 2016) and PSHA (e.g., Field *et al.*, 2008, 2013; Gerstenberger *et al.*, 2016). This study develops a new PSHA approach and emphasizes the impact of time dependency, that is, the determination of time-independent seismicity rate and selection of ground-motion prediction equations (GMPEs) which follow the procedure and parameters of the Taiwan Earthquake Model (TEM)-hazard map (named TEM PSHA2015 by Wang, Chan, *et al.*, 2016). The adaption of time-independent parameters from TEM PSHA2015 allows us to directly compare the impact of our time-dependent functions. For long- and short-term time-dependent factors, our model includes the Brownian passage time (BPT;

*Now at Nuclear Power Division, Taiwan Power Company, Taiwan.

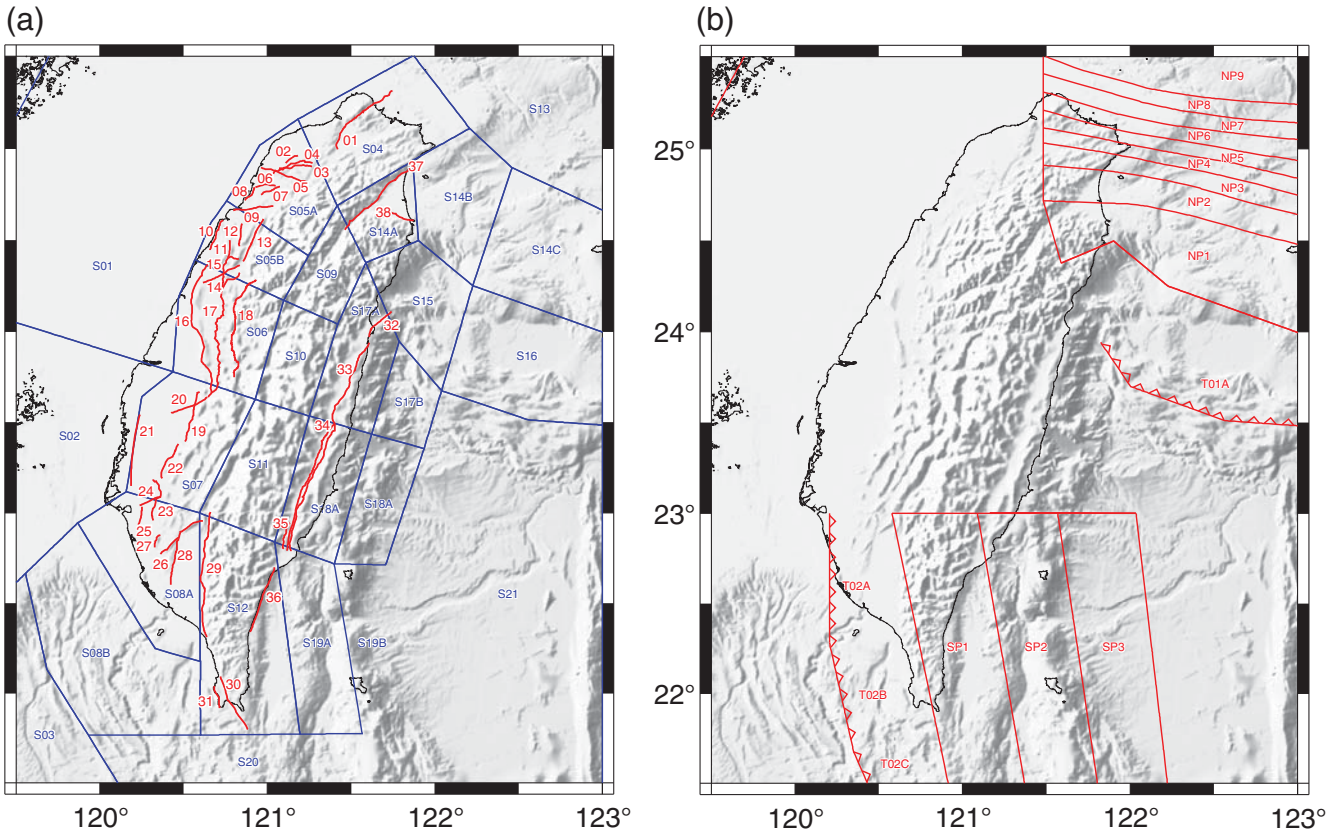

Figure 1. Distribution of (a) shallow areas and seismogenic structures and (b) subduction interplate and intraplate sources. The geometry and corresponding parameters of each source are from Wang, Chan, *et al.* (2016).

Ellsworth *et al.*, 1999) and the rate-and-state friction law (Dieterich, 1994), respectively. In this study, we demonstrate the temporal evolution of seismic hazards in Taiwan and test the credibility of our model.

Methodology and Procedure

A PSHA requires an earthquake occurrence rate for each seismogenic source and appropriate GMPEs (Cornell, 1968; McGuire, 1976). In the following sections, we detail how to calculate a time-dependent seismicity rate by combining the background seismicity model and long- and short-term rate evolutions, as well as how to assess seismic hazard by incorporating GMPEs that describe the path effect and site amplification.

The Background Seismicity Model

To obtain the background seismicity model, we utilized the database of the TEM, which provided the first official version of the seismic-hazard map of Taiwan (Wang, Chan, *et al.*, 2016). In this database, the seismogenic sources in and around Taiwan are classified into three categories: (1) shallow-background area sources, (2) seismogenic structure sources (i.e., specific faults), and (3) subduction-zone sources (Fig. 1). We followed the procedure of the TEM PSHA2015 to estimate the seismicity rate model for each source based on the earthquake catalog and the geological evidence associated with seismogenic structures. Below, we briefly summarize the seismic sources of these three categories.

Shallow-Background Area Sources. Earthquakes with focal depths shallower than 30 km and ruptures that cannot be associated with a specific fault were considered shallow-background area sources in the TEM database. There are 28 subregions (areas) defined in the shallow-background area sources based on the tectonic framework of Taiwan, the neotectonic architecture, Bouguer gravity anomalies, and the regional geological setting (Fig. 1a; Cheng *et al.*, 2015). For describing the seismic occurrence rate of these sources, the truncated model (Cosentino *et al.*, 1977) is implemented (Youngs and Coppersmith, 1985). We implemented the parameters determined by the TEM PSHA2015 (Wang, Chan, *et al.*, 2016) based on the best-fit to the observations of the complete part of the earthquake catalog determined by Chan *et al.* (2013). The estimated *b*-value of 1.07 was utilized uniformly in the all areas to individually assess the corresponding *a*-value of each area (Table 1). The *a*- and *b*-values in TEM PSHA2015 were estimated by a least-squares regression rather than a maximum-likelihood estimation as suggested by previous studies (Aki, 1965, and references therein). However, the revision adopting maximum likelihood is suggested in the next generation of the TEM-hazard map.

Table 1
a- and *b*-Values of the 28 Shallow Area Sources Estimated Using the Truncated Exponential Model Determined by Wang, Chan, *et al.* (2016)

Area	*a*-value	*b*-value
S01	3.69 (±0.103)	1.07 (±0.053)
S02	4.01 (±0.102)	1.07 (±0.053)
S03	3.66 (±0.117)	1.07 (±0.053)
S04	3.17 (±0.198)	1.07 (±0.053)
S05A	3.57 (±0.201)	1.07 (±0.053)
S05B	4.32 (±0.052)	1.07 (±0.053)
S06	4.63 (±0.052)	1.07 (±0.053)
S07	4.72 (±0.087)	1.07 (±0.053)
S08A	4.14 (±0.061)	1.07 (±0.053)
S08B	3.74 (±0.171)	1.07 (±0.053)
S09	3.98 (±0.144)	1.07 (±0.053)
S10	4.80 (±0.172)	1.07 (±0.053)
S11	4.63 (±0.082)	1.07 (±0.053)
S12	4.84 (±0.048)	1.07 (±0.053)
S13	4.37 (±0.136)	1.07 (±0.053)
S14A	4.34 (±0.163)	1.07 (±0.053)
S14B	4.92 (±0.047)	1.07 (±0.053)
S14C	4.79 (±0.123)	1.07 (±0.053)
S15	5.33 (±0.076)	1.07 (±0.053)
S16	5.56 (±0.108)	1.07 (±0.053)
S17A	5.21 (±0.053)	1.07 (±0.053)
S17B	4.42 (±0.141)	1.07 (±0.053)
S18A	4.91 (±0.055)	1.07 (±0.053)
S18B	4.58 (±0.080)	1.07 (±0.053)
S19A	5.16 (±0.134)	1.07 (±0.053)
S19B	4.60 (±0.101)	1.07 (±0.053)
S20	4.53 (±0.110)	1.07 (±0.053)
S21	5.12 (±0.142)	1.07 (±0.053)

Specific Fault Sources. The TEM-specific fault database is based on the seismogenic structure parameters determined by Shyu *et al.* (2016), which combines active fault and blind fault data from published active tectonic research and new field survey results. The database includes 38 seismogenic structures near the surface (Fig. 1a). Possible maximal magnitude produced by each structure was estimated by the empirical magnitude–fault area relationship (Wells and Coppersmith, 1994). Although the Wells and Coppersmith (1994) model is obsolete and has been superseded by many modern empirical models and does not provide a good magnitude estimation for large megathrust earthquakes (e.g., Stirling *et al.*, 2013), Wang, Lee, *et al.* (2016) confirmed that the model only produces trivial differences (mostly within ±0.2) in the maximal magnitudes estimated from Yen and Ma (2011). The seismic occurrence rate of the characteristic earthquakes for each source was evaluated using the ratio of slip rate and average fault slip during a characteristic earthquake. The parameters of each specific fault source are listed in Table 2.

Subduction-Zone Sources. TEM also adopts the models of the Ryukyu and Manila subduction sources from Cheng *et al.* (2007), which defines 4 interplate and 12 intraplate sources based on the geometry of the subducted plates and their isodepth contours (Fig. 1b). The interplate earthquakes are generally attributed to ruptures on a defined megathrust interface. The intraplate earthquakes, which occur within a subduction slab, generally cannot be attributed to a specific fault source. The corresponding source parameters for interplate and intraplate sources are listed in Tables 3 and 4, respectively (Wang, Chan, *et al.*, 2016).

The Long-Term Renewal Model

To model long-term renewal earthquake probabilities, we adopted the BPT model into our analysis. This model was proposed and implemented by Ellsworth *et al.* (1999) in their "Working Group on California Earthquake Probabilities" study, and has been applied to other renewal seismic-hazard models, including the National Seismic Hazard Maps for Japan (Fujiwara, 2014). The distribution expressing density function (DF) in the BPT model is as follows:

$$\mathrm{DF} = \left(\frac{\mu}{2\pi\alpha^2 t^3}\right)^{1/2} \exp\left(-\frac{(t-\mu)^2}{2\alpha^2\mu t}\right), \tag{1}$$

in which μ is the mean recurrence interval, t is the time elapsed since the last rupture of the event, and α is the aperiodicity, which is usually between 0.3 and 0.7. We first assumed a fixed α of 0.5 and then discussed hazard level deviation within a credible range of this parameter.

To obtain the occurrence time of the last rupture on each specific fault source, we utilized the TEM historical earthquake database to obtain the occurrence time and the corresponding sources of past ruptures. To quantify the earthquake probability, we followed the procedure of Erdik *et al.* (2004) to estimate the earthquake probability as follows:

$$P(t, \Delta t) = \frac{\int_t^{t+\Delta t} f(t)dt}{\int_t^{\infty} f(t)dt}. \tag{2}$$

$P(t, \Delta t)$ describes the earthquake probability within the next Δt years when no earthquake has occurred in the past t years; $f(t)$ is the seismicity DF, presented by the BPT model in equation (1). With the time elapsed since the last rupture and the averaged recurrence intervals for the fault, the BPT distribution provides rupture probabilities. Because the average earthquake recurrence intervals in the TEM-specific fault database (Table 2) are usually long (from decades to millennia), the impact of the earthquake probability from the BPT models only becomes significant in long-term periods (i.e., after a long time has elapsed since the last earthquake).

The Short-Term Renewal Model

We evaluated the short-term rate evolution using coulomb stress changes (ΔCFS) of previous earthquakes and the rate-and-state friction model (Dieterich, 1994). For ΔCFS, the constant apparent friction law (Cocco and Rice, 2002) is defined as follows:

$$\Delta\mathrm{CFS} = \Delta\tau + \mu'\Delta\sigma_n, \tag{3}$$

Table 2
Source Parameters of the 38 Seismogenic Structures Identified by Taiwan Earthquake Model (TEM; Shyu *et al.*, 2016)

ID	Name	Rake (°)	Dip (°)	Depth Max (km)	M_w Max	Displacement (m)	Slip Rate (mm/yr)	Recurrence Interval (yrs)
1	Shanchiao fault	−90	60	13.76	7.0	1.33	1.85 (±0.76)	511–1220
2	Shuanglienpo structure	90	45	5.00	6.2	0.67	0.25 (±0.17)	1595–8375
3	Yangmei structure	90	60	3.00	6.0	0.59	0.38 (±0.26)	921–4538
4	Hukou fault	90	30	10.00	6.8	1.15	1.16 (±0.84)	575–3593
5	Fengshan river strike-slip structure	0	85	13.85	6.7	0.96	3.61 (±2.41)	159–800
6	Hsinchu fault	90	45	10.00	6.4	0.81	0.70 (±0.46)	692–3375
7	Hsincheng fault	90	30	12.86	6.6	0.99	1.80 (±1.20)	330–1650
8	Hsinchu frontal structure	90	30	10.00	6.4	0.85	2.80 (±1.86)	182–904
9	Touhuanping structure	0	85	12.00	6.5	0.78	0.14	5571–5571
10	Miaoli frontal structure	90	30	10.00	6.7	1.08	3.60 (±2.40)	180–900
11	Tunglo structure	90	30	3.50	6.0	0.59	1.08 (±0.72)	327–1638
12	East Miaoli structure	90	30	4.00	6.2	0.69	1.60 (±1.06)	259–1277
13	Shihtan fault	90	75	10.80	6.6	0.96	1.86 (±1.24)	308–1548
14	Sanyi fault	90	15	14.85	7.0	1.44	1.86 (±1.23)	466–2322
15	Tuntzuchiao fault	0	85	14.79	6.6	0.88	1.00 (±0.68)	523–2666
16	Changhua fault	90	45	12.00	7.6	2.41	3.40 (±2.26)	425–2132
17	Chelungpu fault	90	15	12.00	7.6	2.44	6.94	351–351
18	Tamaopu–Shuangtung fault	90	30	6.00	7.0	1.34	2.00 (±1.34)	401–2030
19	Chiuchiungkeng fault	90	30	12.00	6.9	1.35	7.20 (±4.80)	112–562
20	Meishan fault	0	85	14.69	6.6	0.87	2.51	346–346
21	Chiayi frontal structure	90	15	12.00	7.3	1.86	6.49 (±4.33)	171–861
22	Muchiliao–Liuchia fault	90	30	12.00	6.8	1.22	5.75 (±1.35)	171–277
23	Chungchou structure	90	30	12.00	6.9	1.30	12.20 (±0.60)	101–112
24	Hsinhua fault	0	85	15.00	6.4	0.65	2.65 (±1.85)	144–812
25	Houchiali fault	90	45	5.00	6.1	0.61	7.07	86–86
26	Chishan fault	45	75	10.80	6.6	0.91	1.10 (±0.36)	623–1246
27	Hsiaokangshan fault	90	30	7.00	6.2	0.70	3.30 (±2.20)	127–636
28	Kaoping River structure	45	75	12.27	6.6	0.89	0.61 (±0.41)	872–4450
29	Chaochou fault	45	75	11.11	7.0	1.43	1.76 (±1.17)	488–2423
30	Hengchun fault	45	75	15.00	6.8	1.14	6.15 (±0.29)	177–194
31	Hengchun offshore structure	90	30	4.00	6.2	0.69	3.65 (±1.11)	144–271
32	Milun fault	45	75	10.00	6.4	0.68	10.15 (±0.04)	66–67
33	Longitudinal Valley fault	45	75	20.00	7.5	2.24	11.35 (±5.75)	130–400
34	Central Range structure	90	45	20.00	7.4	2.02	7.28 (±1.77)	223–36
35	Luyeh fault	90	45	5.00	6.2	0.69	6.34 (±0.17)	105–111
36	Taimali coastline structure	45	75	10.55	6.7	1.11	7.32 (±1.46)	126–189
37	Northern Ilan structure	−90	60	9.41	6.8	1.00	3.29 (±2.25)	180–961
38	Southern Ilan structure	−90	60	11.25	6.4	0.64	5.48 (±0.64)	104–131

in which $\Delta\tau$ is the shear stress change along the slip vector, μ' is the apparent friction coefficient, and $\Delta\sigma_n$ is the normal stress change on the receiver plane. A positive ΔCFS could trigger consequent earthquakes, whereas a stress drop inhibits its seismic activity in the future.

Table 3
Source Parameters for Interplate Subduction-Zone Sources Determined by Wang, Chan, *et al.* (2016)

Source	Dip (°)	M_{max}	Length (km)	Width (km)	Slip Rate (mm/yr)
T01A	20 (±2)	8.0 (±0.2)	138.69	102.3	40 (±10)
T02A	24 (±2)	7.5 (±0.2)	79.12	54.1	8 (±4)
T02B	24 (±2)	7.5 (±0.2)	69.06	54.1	8 (±4)
T02C	24 (±2)	7.5 (±0.2)	81.42	54.1	8 (±4)

Following the procedure of TEM, we adopted the seismicity rates of the characteristic magnitudes (M_{max}) for the sources.

The coulomb stress calculation for each seismogenic source requires receiver plane parameters, that is, geometry and the preferred rupture rake. For specific fault sources, we smoothed the fault surface alignments, segmented each alignment into several subfaults, calculated ΔCFS on each subfault, and recorded the maximum ΔCFS. For shallow-background area sources, we calculated ΔCFS at each edge, in the centroid, and at points in between the edges and the centroid. The focal mechanism of the largest earthquake in each area is assumed to be a receiver plane to calculate the maximum ΔCFS. With such settings, the short-term renewal model suggests that any subsequent earthquake will tend to occur at the point with the highest ΔCFS. Because earthquakes with small magnitudes and/or

Table 4
Source Parameters for Intraplate Subduction-Zone Sources Determined by Wang, Chan, *et al.* (2016)

Source	m_0	a-value	b-value	m_u
NP1	5.0	4.20	0.91	7.7 (±0.2)
NP2	5.0	3.57	0.80	7.7 (±0.2)
NP3	5.0	3.54	0.87	7.7 (±0.2)
NP4	5.0	2.68	0.73	7.8 (±0.2)
NP5	5.0	3.07	0.94	7.8 (±0.2)
NP6	5.0	3.26	0.96	7.8 (±0.2)
NP7	5.0	2.46	0.73	7.8 (±0.2)
NP8	5.0	3.73	1.04	7.8 (±0.2)
NP9	5.0	3.61	0.91	7.8 (±0.2)
SP1	5.0	3.07	0.76	7.7 (±0.2)
SP2	5.0	3.76	0.83	7.8 (±0.2)
SP3	5.0	3.72	0.88	7.8 (±0.2)

We adopted the truncated exponential model (Cosentino *et al.*, 1977) for the sources to represent the seismicity rate. m_u represents the maximal magnitude of the sources.

earthquakes that occurred far in the past do not result in relevant rate perturbations (Catalli *et al.*, 2008; Chan *et al.*, 2013), we only implemented the earthquakes with $M_w \geq 5.5$ and that occurred within three years of the target time for the renewal hazard assessments. It is worth mentioning that the coulomb stress-change model only determines the qualitative trend of the seismicity rate.

To calculate the temporal change in seismicity rate, we applied the rate-and-state friction model together with the coulomb stress changes from Chan *et al.* (2010). The seismicity rate evolution $\Delta R(M,x,t)$ was evaluated using the stress change by the nth earthquake of $\Delta\mathrm{CFS}_n(x)$ at the site (x) as a function of magnitude (M) and time (t) as follows:

$$\Delta R(M,x,t) = \frac{\lambda(M,x)}{\left[\frac{\lambda(M,x)}{\Delta R_{n-1}(M,x)}\exp\left(-\frac{\Delta\mathrm{CFS}_n(x)}{A\sigma}\right)-1\right]\exp\left(-\frac{t-t_n}{t_{na}}\right)+1}, \quad (4)$$

in which $\lambda(M,x)$ is the long-term seismicity rate, $\Delta R_{n-1}(M,x)$ is the short-term rate change just before the occurrence of the nth earthquake (i.e., $\Delta R_0 = \lambda(M,x)$), and $A\sigma$ is a constitutive parameter of the model. We first assumed $A\sigma = 0.3$ and then discussed its influence on the calculations, t_n is the occurrence time of the nth earthquake, and t_{na} is the aftershock duration, assumed to be a function of the magnitude defined by Burkhard and Grünthal (2009). The rate-and-state friction model describes rate evolution during an aftershock period (approximately months to years), which is a relatively short period in comparison with the earthquake recurrence intervals from the BPT model (approximately decades to millennia).

Ground-Motion Prediction Equations

In addition to the reliable seismic rate model of seismogenic sources, another key factor for the PSHA application is introducing the path effect and site amplification through GMPEs. The GMPEs published by Lin and Lee (2008) and Lin (2009) are the most comprehensive and broadly accepted for crustal and subduction earthquakes, respectively, in Taiwan. We followed the procedure of the TEM PSHA2015 and implemented GMPEs by Lin (2009) for the shallow-background area and specific fault sources, and GMPEs by Lin and Lee (2008) for the subduction-zone sources. The GMPE applications are truncated at two standard deviations. We are aware that epistemic uncertainties (Scherbaum and Kuehn, 2011; Bommer, 2012) in implementing several GMPEs through a logic tree are important, and truncating three standard deviations is common in GMPE applications. To make our model comparable to the TEM PSHA2015 model, we decided to follow the same parameters implemented by the TEM PSHA2015 (Wang, Chan, *et al.*, 2016). We will suggest that TEM revise these parameters in the next version of the hazard map.

Results

Based on the above-mentioned parameters, we modeled the PSHA in Taiwan at various time snapshots (Fig. 2a–d), described as follows.

First, we present a classic time-independent hazard map (Fig. 2a) as the basis of our seismic-hazard model. This model is essentially identical to the current version of the TEM PSHA2015 (Wang, Chan, *et al.*, 2016), because they share the same source parameters and model settings. It is clear that high hazard areas within Taiwan are mainly dominated by active faults with high slip rates and short earthquake recurrence intervals, for example, the Changhua fault (number 16), the Chelungpu fault (number 17), the Chungchou structure (number 23), and the Longitudinal Valley fault (number 33). In contrast, low hazard levels are in areas with lower seismicity rates and low a values (Table 1), for example, the Central Ranges in S09 and northern Taiwan in S04 and S05A.

Figure 2b–d shows results from our renewal models at different time snapshots, after incorporating both the long-term BPT and the short-term rate-and-state friction models. In comparison with the time-independent hazard map (Fig. 2a), our model shows a significantly higher hazard level in the vicinity of the Chelungpu fault immediately prior to the 1999 M_w 7.6 Chi-Chi earthquake (Fig. 2b). The ascending hazard (from 0.57g to 0.79g) near the Chelungpu fault (number 17 in Table 5) is attributed to an increase rupture probability of the fault (+110.2%) as compared to the BPT model due to the long time elapsed since its last rupture (Table 5), together with a coulomb stress increase caused by the 1998 M_w 5.7 Rueyli earthquake (the star in Fig. 2b). A higher hazard (from 0.69g to 0.78g) is also expected near the Muchiliao–Liuchia fault (number 22); its rupture probability increased 32.5%, as the time elapsed since its last event in 1862 is closer to its mean recurrence interval of 212 yrs (Table 5). In contrast, a lower hazard (from 0.56g to 0.44g) near the Shitan and the Tuntzuchiao faults (numbers 13 and

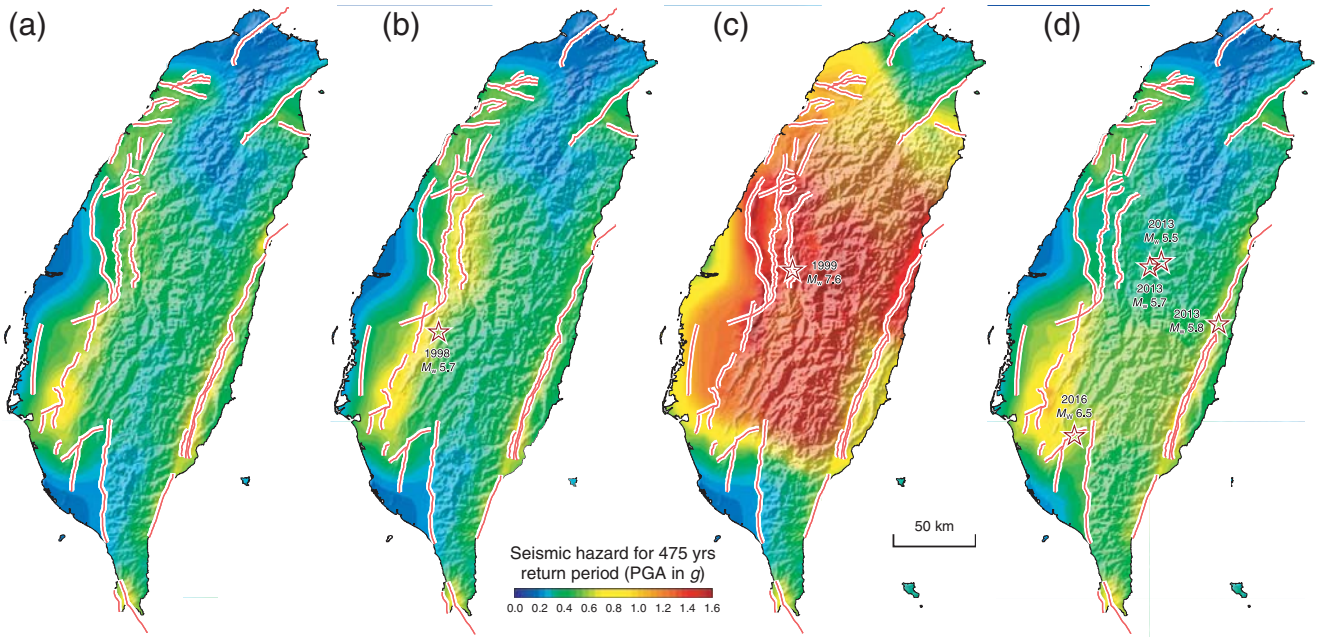

Figure 2. (a) Time-independent and (b) time-dependent probabilistic seismic hazards immediately before the 1999 Chi-Chi earthquake, (c) immediately after the Chi-Chi earthquake, and (d) in the middle of 2016. The implemented earthquakes for short-term rate evolution for each time snapshot are denoted by stars.

15, respectively, in Table 5) is associated with the short time elapsed since the 1935 M_L 7.1 Hsinchu–Taichung earthquake, during which both of these two faults ruptured.

For the model time period immediately following the Chi-Chi earthquake in September 1999, we evaluated the coulomb stress change resulting from the M_w 7.6 Chi-Chi earthquake based on the detailed slip dislocation model by Johnson and Segall (2004). Our renewal model (Fig. 2c) shows that the stress enhanced by the Chi-Chi event significantly increased rupture probabilities of several neighboring faults, for example, the Changhua (number 16), Tamaopu–Shuangtung (number 18), Chiuchiungkeng (number 19), and Meishan (number 20) faults, and the earthquake probabilities of the neighboring area sources. The elevated hazard level in central Taiwan (e.g., from 0.80g to 1.61g at the epicenter of the Chi-Chi earthquake) after the Chi-Chi earthquake is evidenced by the occurrence of the widespread aftershocks, including some with $M_w \geq 6.0$ (Chang *et al.*, 2000). The rupture probability of the Chelungpu fault at this time snapshot is close to zero (Table 5).

We also assessed seismic hazard in the coming future by further incorporating the sequential coulomb stress changes from significant earthquake events in recent years (Fig. 2d). For evaluating short-term rate evolution, we considered the coulomb stress change by the earthquakes with $M_w \geq 5.5$ that have occurred since 2013 (represented as stars in Fig. 2d). For

Table 5

Rupture Probabilities and Relative Rate Differences Determined by Different Models at the Time Snapshots of 1999 and 2016 Based on Corresponding Recurrence Intervals and Time Elapsed Since the Last Event

				Year 1999			Year 2016		
Fault Name	ID	Recurrence Interval (yrs)	Percentage in 50 yrs (Poisson)	Time Elapse	Rate (%)	Rate Change (%)	Time Elapse	Rate (%)	Rate Change (%)
Shihtan fault	13	516	97.9	66	0.1	−99.0	81	0.2	−97.7
Tuntzuchiao fault	15	880	96.4	66	0.0	−100.0	81	0.0	−100.0
Changhua fault	16	303	95.6	153	18.3	22.8	168	20.0	35.2
Chelungpu fault	17	371	12.6	415	24.7	110.2	17	0.0	−99.9
Meishan fault	20	347	91.8	95	5.0	−64.8	110	6.8	−51.1
Muchiliao–Liuchia fault	22	212	89.7	139	32.5	66.6	154	34.1	76.8
Hsinhua fault	24	245	87.5	55	6.0	−69.7	70	9.4	−51.7
Milun fault	32	189	23.2	50	13.6	−44.8	65	19.2	−19.6
Longitudinal Valley fault	33	189	23.2	50	13.6	−44.8	65	19.2	−19.6

The time-dependent and time-independent rates are estimated according to the Brownian passage time (BPT) and Poisson models, respectively. The locations of active faults are presented in Figure 1. Note that for the Chelungpu fault, we obtained two time-dependent rates before and after the Chi-Chi earthquake, respectively.

Table 6
Determined Rupture Probabilities Based on Different Aperiodicity Values at the Time Snapshots of 2016

Fault Name	ID	Recurrence Interval (yrs)	Time Elapse (yrs)	$\alpha = 0.3$ (%)	$\alpha = 0.5$ (%)	$\alpha = 0.7$ (%)
Shihtan fault	13	516	66	0.0	0.2	2.7
Tuntzuchiao fault	15	880	66	0.0	0.0	0.1
Changhua fault	16	303	153	14.2	20.0	20.8
Chelungpu fault	17	371	415	0.0	0.0	0.5
Meishan fault	20	347	95	0.6	6.8	13.4
Muchiliao–Liuchia fault	22	212	139	40.5	34.1	29.9
Hsinhua fault	24	245	55	1.1	9.4	18.2
Milun fault	32	189	50	6.3	19.2	27.0
Longitudinal Valley fault	33	189	50	6.3	19.2	27.0

the 6 February 2016 M_w 6.5 Meinong earthquake, we implemented the detailed slip dislocation model from the joint inversion of Global Positioning System and teleseismic and near-field strong-motion data by Lee (2016). The geometry of the rupturing fault and the slip magnitude for other earthquakes are estimated based on their moment magnitudes and the scaling law of Yen and Ma (2011). Figure 2d shows the results from our renewal model in the middle of 2016. Significant seismic-hazard elevation in southwest Taiwan (from 1.02g before the 1999 Chi-Chi earthquake to 1.18g following it) is attributed to a rupture probability increase on the Muchiliao–Liuchia fault (number 22, +76.8%) due to the long time elapsed since its last event (154 yrs) (Table 5) together with a coulomb stress increase from the 2016 Meinong earthquake. Lee *et al.* (2017) suggests that although the 2016 Meinong earthquake partially diminishes the seismic-hazard potential in southern Taiwan, more than ~80% of the hazard potential from fault sources have not yet been released. Additionally, it is notable that the hazard level in the area close to the Chelungpu fault is still lower than the level in other models due to its low rupture probability from the short time elapsed since the Chi-Chi earthquake in 1999. Compared to the hazard map before the 1999 Chi-Chi earthquake (Fig. 2b), the seismic hazard has increased steadily (from 0.56g to 0.67g) along the Longitudinal Valley fault (number 33). The elevated hazard level can be attributed to the rapid rupture probability increase of the Longitudinal Valley fault (from 13.6% to 19.2%) due to its short average recurrence interval (189 yrs, Table 5). However, our renewal model still suggests the current rupture probability of the fault is 19.2%, which is 19.6% lower than that predicted by the time-independent model, a result of the short time elapsed since the 1951 Longitudinal Valley earthquake sequence.

Discussion

The Sensitivity of Model Parameters

Because we applied the BPT distribution (shown in equation 1) to our renewal model to constrain the time-dependent long-term change of earthquake probabilities for specific fault sources, the aperiodicity value (α), which is usually between 0.3 and 0.7, becomes an important factor in controlling the temporal change of earthquake probability. To test the deviations contributed by α, we evaluated the rupture probabilities for the specific fault sources using the two end members 0.3 and 0.7, respectively (Table 6). The test results yield trivial changes in the PSHA model, as less than 2% of the total area is affected by the hazard level change for more than 0.1g (Fig. 3). The deviation is mainly located along the Milun (number 32) and Longitudinal Valley faults (number 33) with maximum probability differences of 20.7% due to the change of α.

In terms of short-term rate evolution, our analysis heavily relies on the rate-and-state friction model and the modeled ΔCFS (shown in equation 4). In our above analyses, the rate-and-state friction model was applied by considering a fixed $A\sigma$ of 0.3 bars. To test the short-term hazard assessment stability related to $A\sigma$, we compared the seismic rates by varying $A\sigma$ from 0.2 to 0.4 bars, corresponding to the boundaries of the physically reasonable ranges (Toda and Stein, 2003, and references therein). When $A\sigma$ was assumed to be between 0.2 and 0.4 bars, differences in the hazard map were found to be insignificant, as only 0.6% of the total area was affected by a hazard level difference of more than 0.1g (Fig. 4). The difference in southwestern Taiwan is associated with the ΔCFS from the 2015 Meinong earthquake (the star in Fig. 4c), because the impact of ΔCFS becomes more significant when a lower $A\sigma$ is assumed.

Our simple tests suggest insensitivity of our assessment to the parameters of aperiodicity values (α) for the BPT and a constitutive parameter ($A\sigma$) of the rate-and-state friction model. Another means to minimize the deviation from epistemic uncertainties is the application of a logic tree to the assessment. We assume weights of 0.2, 0.6, and 0.2 for α of 0.3, 0.5, and 0.7, respectively, and weights of 0.2, 0.6, and 0.2 for $A\sigma$ of 0.2, 0.3, and 0.4, respectively. In comparison to the hazard of an assuming fixed α of 0.5 and $A\sigma$ of 0.3, the difference in hazard level is irrelevant, because the difference is less than 0.05g for all calculation nodes (Fig. 5).

The Model Applications

The time-dependent rate models previously mentioned are analyzed for the time snapshots of our interests and are snapshots that we believe could best demonstrate the applicability of this renewal model. For example, we assessed probabilistic seismic hazard in the middle of 2016 considering both long-term and short-term factors and obtained a higher hazard level in southwestern Taiwan (Figs. 2d and 6a). Such hazard elevation is attributed to a short-term rate increase following

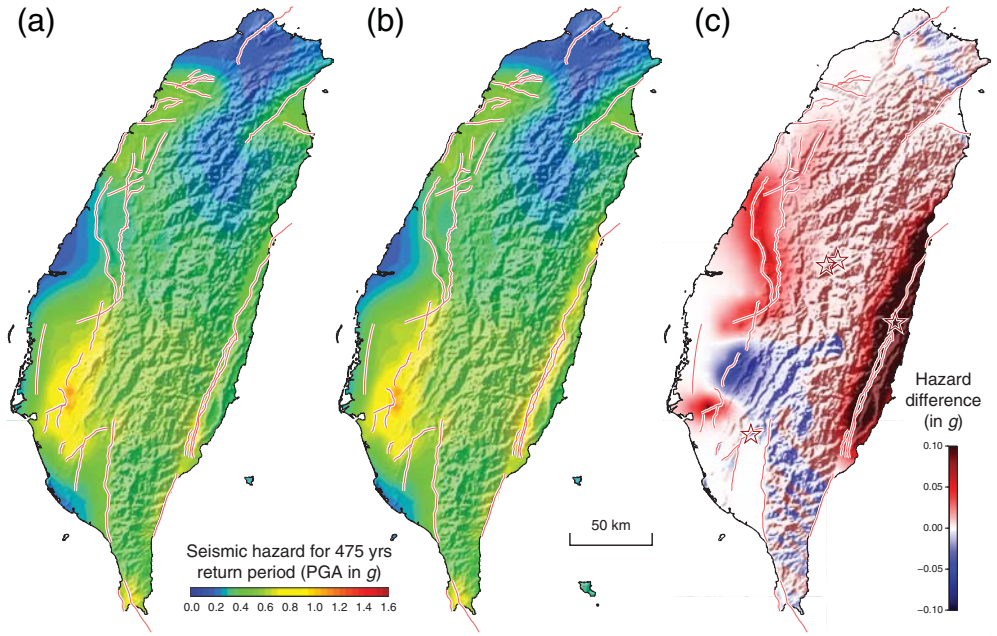

Figure 3. The seismic-hazard maps considering the aperiodicity values (α) of (a) 0.3 and (b) 0.7, and (c) the difference between each. The implemented earthquakes for short-term rate evolution are denoted by stars.

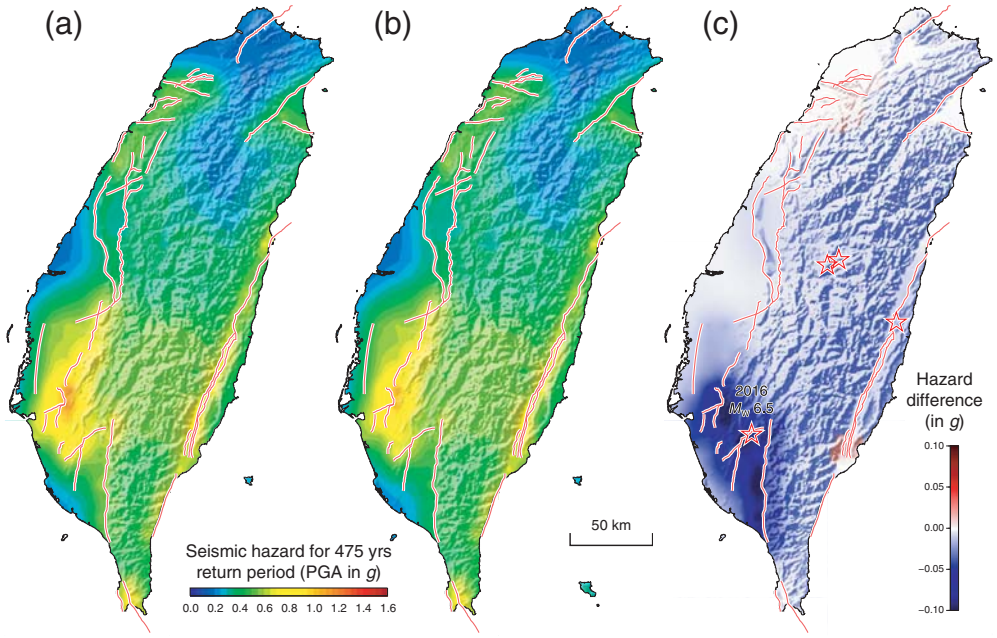

Figure 4. The seismic-hazard maps considering constitutive parameters ($A\sigma$) of (a) 0.2 and (b) 0.4, and (c) the difference between each. The implemented earthquakes for short-term rate evolution are denoted by stars.

the 2016 M_w 6.5 Meinong earthquake and can be associated with occurrence of subsequent aftershocks in this region.

Based on short-term factors through the rate-and-state friction model, our assessment provides an adequate basis for rapid evaluations and response after a devastating earthquake, for example, victim relocation and sheltering. In an area such as Taiwan with a high tectonic stressing rate, the impact of a short-term rate change in the interplate environment becomes trivial when assessing periods that are longer (see Fig. 6b–d). Considering aftershock durations of ~1–2 yrs (Burkhard and Grünthal, 2009), the short-term rate evolution is insignificant when assessing periods longer than 10 yrs (Fig. 6c,d), and the outcomes are close to the time-independent hazard map (Fig. 2a). Thus, long-term factors are crucial for the applications of long-term seismic-hazard management in the interplate environment.

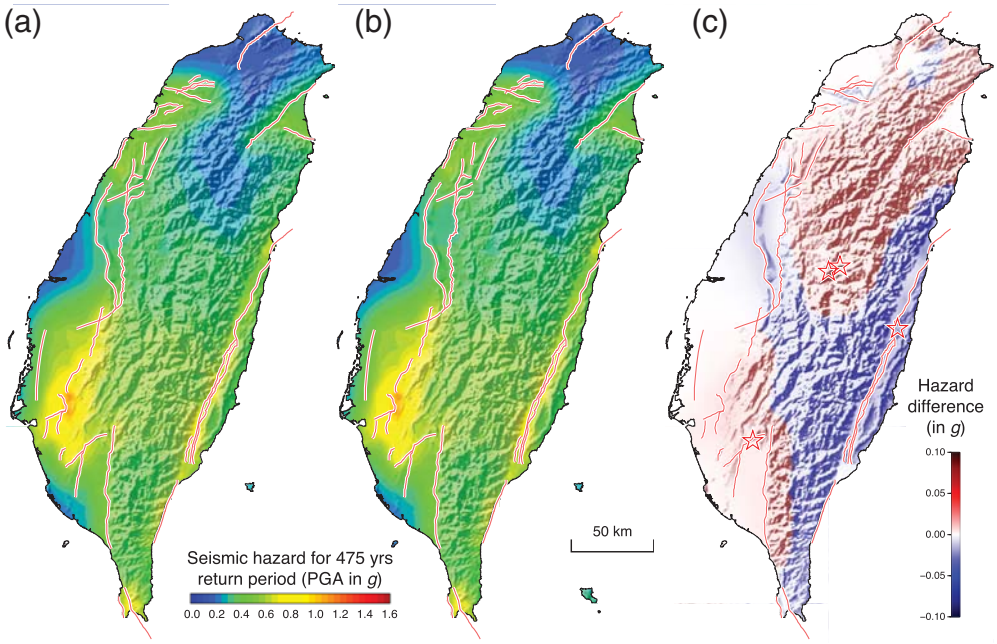

Figure 5. The seismic-hazard maps considering (a) logic tree and (b) fixed parameters for aperiodicity values and a constitutive parameter, and (c) the difference between each. A detailed setting of the logic tree is described in The Sensitivity of Model Parameters section. The implemented earthquakes for short-term rate evolution are denoted by stars.

For the intraplate environment, where the ongoing tectonic stressing rate is significantly lower than the rate in the interplate region, the impact from the rate-and-state friction model would last much longer, that is, several decades to even several hundred years. The level of the seismic hazard would remain high for a significant period after one major intraplate earthquake, even though the mean recurrence interval of active faults in the intraplate regions is generally several thousand to more than ten thousand years. However, the contribution from the BPT-based long-term model may become less significant in the intraplate region due to the long recurrence interval of fault rupture. We, therefore, suggest that the short-term model in the intraplate region could play an important role in deterministic-based hazard and risk assessments or the revision of building codes after a major intraplate earthquake, for example, the 1976 Tangshan earthquake and the New Madrid earthquake sequences in 1811 and 1812.

Suggestion for the Next Generation of the TEM Hazard Map

Time-dependent models have been incorporated into several PSHA applications in different regions, for example, California (Field *et al.*, 2008, 2013) and New Zealand (Gerstenberger *et al.*, 2016). Our approach draws on the advantages of time dependence and incorporating long- and short-term models and provides earthquake probability constraints, which are more detailed than any of the models could provide on their own for Taiwan. The insight of the current study offers the TEM with an adequate basis for revision of the next hazard map.

We followed the suggestion of Chan (2016) to incorporate both time-independent and time-dependent factors in our model. This model includes a single approach for each time factor, that is, the TEM PSHA2015 model (Wang, Chan, *et al.*, 2016) for the time-independent factor, the BPT distribution (Ellsworth *et al.*, 1999) for the time-dependent long-term factor, and the rate-and-state friction law (Dieterich, 1994) for the time-dependent short-term factor. Our model provides an option for each time factor. However, as Rhoades *et al.* (2016) have suggested, an approach with better forecasting ability occurs if multiple models jointly illustrate seismic behavior of each time factor. To optimize an approach with multiple models requires additional earthquake forecasting tests, which is beyond the scope of this study.

Conclusions

Although the traditional PSHAs (McGuire, 1976, and references therein) typically model earthquake occurrence as a Poisson process, recent studies have emphasized the importance of renewed seismic activity. To compensate for this deficiency of traditional PSHAs, we propose an approach that evaluates the long-term earthquake probability by implementing time elapsed since last events and recurrence intervals of specific faults, and short-term rate change due to coulomb stress changes following earthquake ruptures.

Our model confirms previous interpretations of seismic hazard in southwestern Taiwan, and it further shows that the hazard level continues to increase. For a time-independent model, several specific fault sources are identified with high slip rates and short earthquake recurrence intervals. Considering long-term rate evolution, the long time elapsed since

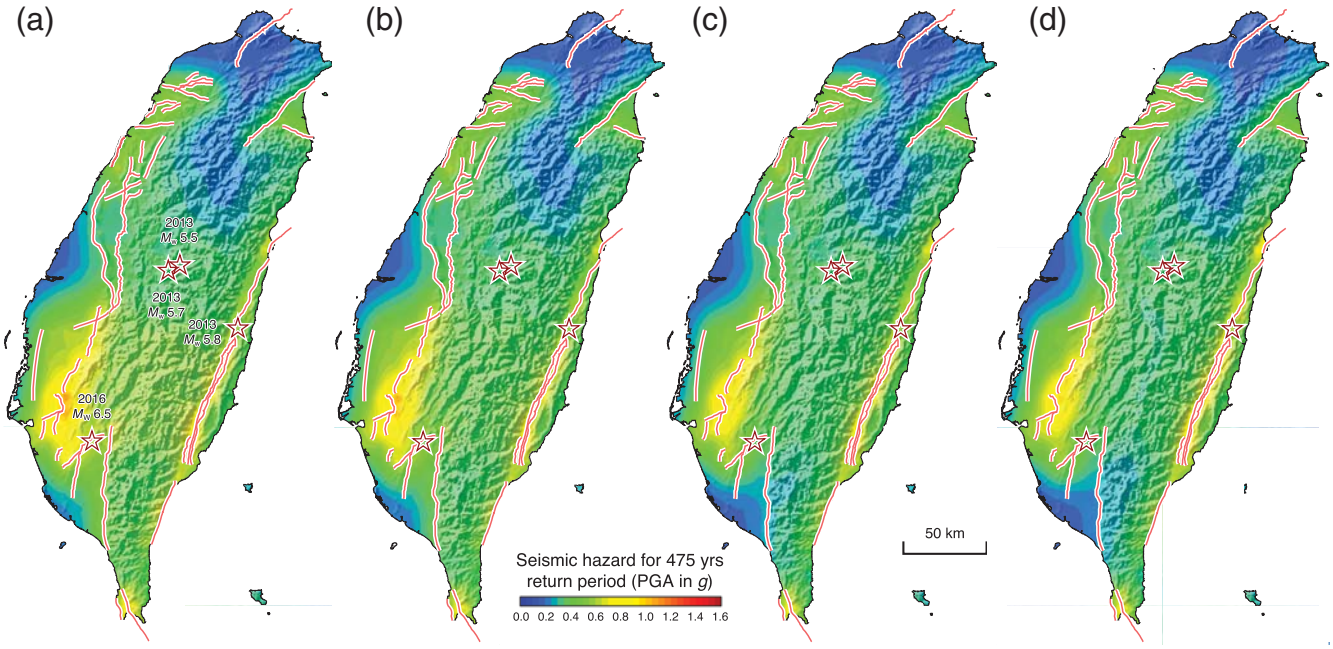

Figure 6. The seismic-hazard maps considering the rate model (a) in the middle of 2016, (b) in 1 yr, (c) in 10 yrs, and (d) in 50 yrs from the middle of 2016. The implemented earthquakes for short-term rate evolution are denoted by stars.

the last rupture on the Muchiliao–Liuchia fault results in a rupture probability increase. For short-term rate perturbation, earthquake probabilities for some seismogenic sources in this region are promoted by the 2016 Meinong earthquake.

Data and Resources

The source parameters of our seismic-hazard model are from the Taiwan Earthquake Model (TEM, http://tec.earth.sinica.edu.tw/TEM/index.php, last accessed February 2016). The earthquake parameters of historical events are obtained from the TEM historical earthquake database (http://tec.earth.sinica.edu.tw/TEM/historic.php?p=5, last accessed December 2014). The focal mechanisms of selected earthquake events were obtained from Broadband Array in Taiwan for Seismology (BATS, http://bats.earth.sinica.edu.tw, last accessed January 2016). The detailed slip dislocation model of the 6 February 2016 M_w 6.5 Meinong earthquake was derived from Shiann-Jong Lee (http://tec.earth.sinica.edu.tw/new_web/upload/news/Conference/20160206meilongEQ/2016-02-06-slip.txt, last accessed June 2016). Our seismic-hazard analysis is calculated using the OpenQuake Engine v.1.0.0 (www.openquake.org, last accessed September 2014).

Acknowledgments

The authors are thankful for the comments from Mark Stirling and one anonymous reviewer, which improved the quality of this study. This work comprises Earth Observatory of Singapore Contribution Number 154. This research is supported by the National Research Foundation Singapore, the Singapore Ministry of Education under the Research Centres of Excellence initiative, and the Ministry of Science and Technology, Taiwan. Y.-T. Lee is grateful for research support from both the Ministry of Science and Technology (MOST) with project Grant Number MOST 103-2116-M-008008-MY3 and the Department of Earth Sciences, National Central University, Taiwan, Republic of China.

References

Aki, K. (1965). Maximum likelihood estimate of b in the formula log $N = a - bM$ and its confidence limits, *Bull. Earthq. Res. Inst. Univ. Tokyo* **43,** 237–239.

Ang, A. H. S., and W. H. Tang (1975). *Probability Concepts in Engineering Planning and Design: Basic Principles*, Vol. 1, Wiley, New York, New York.

Bommer, J. J. (2012). Challenges of building logic trees for probabilistic seismic hazard analysis, *Earthq. Spectra* **28,** no. 4, 1723–1735.

Burkhard, M., and G. Grünthal (2009). Seismic source zone characterization for the seismic hazard assessment project PEGASOS by the Expert Group 2 (EG 1b), *Swiss J. Geosci.* **102,** no. 1, 149–188.

Catalli, F., M. Cocco, R. Console, and L. Chiaraluce (2008). Modeling seismicity rate changes during the 1997 Umbria-Marche sequence (central Italy) through a rate- and state-dependent model, *J. Geophys. Res.* **113,** no. B11301, doi: 10.1029/2007JB005356.

Chan, C. H. (2016). Importance of three-dimensional grids and time-dependent factors for the applications of earthquake forecasting models to subduction environments, *Nat. Hazards Earth Syst. Sci.* **16,** 2177–2187, doi: 10.5194/nhess-16-2177-2016.

Chan, C. H., M. B. Sørensen, D. Stromeyer, G. Grünthal, O. Heidbach, A. Hakimhashemi, and F. Catalli (2010). Forecasting Italian seismicity through a spatio-temporal physical model: Importance of considering time dependency and reliability of the forecast, *Ann. Geophys.* **53,** no. 3, doi: 10.4401/ag-4761.

Chan, C. H., Y. M. Wu, C. T. Cheng, P. S. Lin, and Y. C. Wu (2013). Time-dependent probabilistic seismic hazard assessment and its application to Hualien City, Taiwan, *Nat. Hazards Earth Syst. Sci.* **13,** 1143–1158, doi: 10.5194/nhess-13-1143-2013.

Chan, C. H., Y. M. Wu, and T. L. Lin (2012). A short term seismic hazard assessment in Christchurch, New Zealand, after the M 7.1, 4 September 2010 Darfield earthquake: An application of a smoothing Kernel and rate-and-state friction model, *Terr. Atmos. Ocean. Sci.* **23,** doi: 10.3319/TAO.2011.09.23.02(T).

Chang, C. H., Y. M. Wu, T. C. Shin, and C. Y. Wang (2000). Relocation of the 1999 Chi-Chi earthquake in Taiwan, *Terr. Atmos. Ocean. Sci.* **11,** no. 3, 581–590.

Cheng, C. T., S. J. Chiou, C. T. Lee, and Y. B. Tsai (2007). Study on probabilistic seismic hazard maps of Taiwan after Chi-Chi earthquake, *J. GeoEng.* **2,** 19–28.

Cheng, C. T., P. S. Hsieh, P. S. Lin, Y. T. Yen, and C. H. Chan (2015). Probability seismic hazard mapping of Taiwan, *Encycl. Earthq. Eng.* doi: 10.1007/978-3-642-36197-5_100-1.

Cocco, M., and J. R. Rice (2002). Pore pressure and poroelasticity effects in coulomb stress analysis of earthquake interactions, *J. Geophys. Res.* **107,** no. B2, 2030, doi: 10.1029/2000JB000138.

Cornell, C. A. (1968). Engineering seismic risk analysis, *Bull. Seismol. Soc. Am.* **58,** 1583–1606.

Cornell, C. A., and S. R. Winterstein (1986). Applicability of the Poisson earthquake-occurrence model, in seismic hazard methodology for the central and eastern United States, *EPRI Res. Rept. NP-4726*, Electric Power Research Institute, Palo Alto, California.

Cosentino, P., V. Ficarra, and D. Luzio (1977). Truncated exponential frequency-magnitude relationship in earthquake statistics, *Bull. Seismol. Soc. Am.* **67,** no. 6, 1615–1623.

Dieterich, J. (1994). A constitutive law for rate of earthquake production and its application to earthquake clustering, *J. Geophys. Res.* **99,** 2601–2618.

Ellsworth, W. L., M. V. Matthews, R. M. Nadeau, S. P. Nishenko, P. A. Reasenberg, and R. W. Simpson (1999). A physically-based earthquake recurrence model for estimation of long-term earthquake probabilities, *U.S. Geol. Surv. Open-File Rept. 99-522*.

Erdik, M., M. Demircioglu, K. Sesetyan, E. Durukal, and B. Siyahi (2004). Earthquake hazard in Marmara region, Turkey, *Soil Dynam. Earthq. Eng.* **24,** no. 8, 605–631, doi: 10.1016/j.soildyn.2004.04.003.

Field, E. H., G. P. Biasi, P. Bird, T. E. Dawson, K. R. Felzer, D. D. Jackson, K. M. Johnson, T. H. Jordan, C. Madden, A. J. Michael, *et al.* (2013). Uniform California Earthquake Rupture Forecast, version 3 (UCERF3)—The time-independent model, *U.S. Geol. Surv. Open-File Rept. 2013-1165*, 97 p., *California Geol. Surv. Special Rept. 228*, and *Southern California Earthquake Center Publication 1792*, http://pubs.usgs.gov/of/2013/1165/ (last accessed May 2017).

Field, E. H., T. E. Dawson, K. R. Felzer, A. D. Frankel, V. Gupta, T. H. Jordan, T. Parsons, M. D. Petersen, R. S. Stein, R. J. Weldon II, *et al.* (2008). The Uniform California Earthquake Rupture Forecast, version 2 (UCERF 2), *U.S. Geol. Surv. Open-File Rept. 2007-1437*.

Fujiwara, H. (2014). Seismic hazard maps for Japan, in *Encyclopedia of Complexity and Systems Science*, Springer, New York, New York, 1–28.

Gardner, J. K., and L. Knopoff (1974). Is the sequence of earthquakes in southern California, with aftershocks removed, Poissonian? *Bull. Seismol. Soc. Am.* **64,** 1363–1367.

Gerstenberger, M. C., D. A. Rhoades, and G. H. McVerry (2016). A hybrid time-dependent probabilistic seismic-hazard model for Canterbury, New Zealand, *Seismol. Res. Lett.* **87,** no. 6, 131–1318, doi: 10.1785/0220160084.

Harris, R. A. (1998). Introduction to special section: Stress triggers, stress shadows, and implications for seismic hazard, *J. Geophys. Res.* **103,** 24,347–24,358.

Johnson, K. M., and P. Segall (2004). Imaging the ramp–décollement geometry of the Chelungpu fault using coseismic GPS displacements from the 1999 Chi-Chi, Taiwan earthquake, *Tectonophysics* **378,** no. 1, 123–139.

Lee, S. J. (2016). Analysis of the source rupture model of Meinong earthquake with M_w 6.4 on February 6, 2016, *TEM 105/02/06 Meinong earthquake (M_L 6.4) conference*, http://tec.earth.sinica.edu.tw/new_web/upload/news/Conference/20160206meilongEQ/2016-02-06-slip.txt (last accessed July 2016).

Lee, Y. T., Y. J. Wang, C. H. Chan, and K. F. Ma (2017). The 2016 Meinong earthquake to TEM PSHA2015, *Terr. Atmos. Ocean. Sci.* doi: 10.3319/TAO.2016.12.28.02.

Lin, P. S. (2009). Ground-motion attenuation relationship and path-effect study using Taiwan data set, *Ph.D. Thesis*, Institute of Geophysics, National Central University, Chung-Li, Taiwan (in Chinese).

Lin, P. S., and C. T. Lee (2008). Ground-motion attenuation relationships for subduction-zone earthquakes in northeastern Taiwan, *Bull. Seismol. Soc. Am.* **98,** no. 1, 220–240, doi: 10.1785/0120060002.

McGuire, R. (1976). FORTRAN computer program for seismic risk analysis, *U.S. Geol. Surv. Open-File Rept. 76-67*, 90 pp.

McGuire, R. (2001). Deterministic vs. probabilistic earthquake hazard and risks, *Soil Dynam. Earthq. Eng.* **21,** 377–384.

Merz, H. A., and C. A. Cornell (1973). Seismic risk analysis based on a quadratic magnitude–frequency law, *Bull. Seismol. Soc. Am.* **63,** 1999–2006.

Omi, T., Y. Ogata, Y. Hirata, and K. Aihara (2015). Intermediate-term forecasting of aftershocks from an early aftershock sequence: Bayesian and ensemble forecasting approaches, *J. Geophys. Res.* **120,** no. 4, 2561–2578.

Rhoades, D. A., M. Liukis, A. Christophersen, and M. C. Gerstenberger (2016). Retrospective tests of hybrid operational earthquake forecasting models for Canterbury, *Geophys. J. Int.* **204,** no. 1, 440–456.

Scherbaum, F., and N. M. Kuehn (2011). Logic tree branch weights and probabilities: Summing up to one is not enough, *Earthq. Spectra* **27,** no. 4, 1237–1251.

Shyu, J. B. H., Y. R. Chuang, Y. L. Chen, Y. R. Lee, and C. T. Cheng (2016). A new on-land seismogenic structure source database from the Taiwan Earthquake Model (TEM) project for seismic hazard analysis of Taiwan, *Terr. Atmos. Ocean. Sci.* **27,** no. 3, doi: 10.3319/TAO.2015.11.27.02(TEM).

Stirling, M., T. Goded, K. Berryman, and N. Litchfield (2013). Selection of earthquake scaling relationships for seismic-hazard analysis, *Bull. Seismol. Soc. Am.* **103,** no. 6, 2993–3011, doi: 10.1785/0120130052.

Toda, S., and R. S. Stein (2003). Toggling of seismicity by the 1997 Kagoshima earthquake couplet: A demonstration of time-dependent stress transfer, *J. Geophys. Res.* **108,** no. B12, 2567, doi: 10.1029/2003JB002527.

Wang, Y. J., C. H. Chan, Y. T. Lee, K. F. Ma, J. B. H. Shyu, and R. J. Rau (2016). Probabilistic seismic hazard assessments for Taiwan, *Terr. Atmos. Ocean. Sci.* **27,** no. 3, 325–340.

Wang, Y. J., Y. T. Lee, C. H. Chan, and K. F. Ma (2016). An investigation of the reliability of the Taiwan earthquake model PSHA2015, *Seismol. Res. Lett.* **88,** no. 2A, doi: 10.1785/0220160085.

Wells, D. L., and K. J. Coppersmith (1994). New empirical relationships among magnitude, rupture length, rupture width, rupture area, and surface displacement, *Bull. Seismol. Soc. Am.* **84,** 974–1002.

Yen, Y. T., and K. F. Ma (2011). Source-scaling relationship for M 4.6–8.9 earthquakes, specifically for earthquakes in the collision zone of Taiwan, *Bull. Seismol. Soc. Am.* **101,** no. 2, doi: 10.1785/0120100046.

Youngs, R. R., and K. J. Coppersmith (1985). Implications of fault slip rates and earthquake recurrence models to probabilistic seismic hazard estimates, *Bull. Seismol. Soc. Am.* **75,** no. 4, 939–964.

Earth Observatory of Singapore
Nanyang Technological University
50 Nanyang Avenue, 639798 Singapore
hantijun@googlemail.com
(C.-H.C., Y.W.)

Institute of Nuclear Energy Research
Atomic Energy Council, Executive Yuan
1000 Wenhua Road, Jiaan Village, Longtan District
Taoyuan City 32546, Taiwan
(Y.-J.W.)

Department of Earth Sciences
National Central University
No. 300, Jhongda Road, Jhongli District
Taoyuan City 32001, Taiwan
(Y.-T.L.)

Manuscript received 5 September 2016;
Published Online 25 September 2017